Solar Phys (2007) 244: 25–43
DOI 10.1007/s11207-007-9020-8

Are CME-Related Dimmings Always a Simple Signature of Interplanetary Magnetic Cloud Footpoints?

C.H. Mandrini · M.S. Nakwacki · G. Attrill · L. van Driel-Gesztelyi · P. Démoulin · S. Dasso · H. Elliott

Received: 2 March 2007 / Accepted: 3 August 2007 / Published online: 27 September 2007

Abstract Coronal dimmings are often present on both sides of erupting magnetic configurations. It has been suggested that dimmings mark the location of the footpoints of ejected flux ropes and, thus, their magnetic flux can be used as a proxy for the flux involved in the ejection. If so, this quantity can be compared to the flux in the associated interplanetary magnetic cloud to find clues about the origin of the ejected flux rope. In the context of this physical interpretation, we analyze the event, flare, and coronal mass ejection (CME) that occurred in active region 10486 on 28 October 2003. The CME on this day is associated with large-scale dimmings, located on either side of the main flaring region. We combine SOHO/Extreme Ultraviolet Imaging Telescope data and Michelson Doppler Imager magnetic maps to identify and measure the flux in the dimming regions. We model the associated cloud and compute its magnetic flux using *in situ* observations from the Magnetometer Instrument and the Solar Wind Electron Proton Alpha Monitor aboard the *Advance Composition Explorer*. We find that the magnetic fluxes of the dimmings and magnetic cloud are incompatible, in contrast

C.H. Mandrini (✉) · M.S. Nakwacki · S. Dasso
Instituto de Astronomía y Física del Espacio, CONICET-UBA, CC. 67, Suc. 28, 1428 Buenos Aires, Argentina
e-mail: mandrini@iafe.uba.ar

G. Attrill · L. van Driel-Gesztelyi
University College London, Mullard Space Science Laboratory, Holmbury St. Mary, Dorking, Surrey, RH5 6NT, UK

L. van Driel-Gesztelyi · P. Démoulin
Observatoire de Paris, LESIA, UMR 8109 (CNRS), 92195 Meudon Principal Cedex, France

L. van Driel-Gesztelyi
Konkoly Observatory of the Hungarian Academy of Sciences, Budapest, Hungary

S. Dasso
Departamento de Física, Facultad de Ciencias Exactas y Naturales, Universidad de Buenos Aires, 1428 Buenos Aires, Argentina

H. Elliott
Southwest Research Institute, 6220 Culebra Road, San Antonio, TX 78238, USA

to what has been found in previous studies. We conclude that, in certain cases, especially in large-scale events and eruptions that occur in regions that are not isolated from other flux concentrations, the interpretation of dimmings requires a deeper analysis of the global magnetic configuration, since at least a fraction of the dimmed regions is formed by reconnection between the erupting field and the surrounding magnetic structures.

Keywords Coronal mass ejections: low coronal signatures · Coronal mass ejections: interplanetary · Magnetic field: photosphere · Magnetic field: interplanetary

1. Introduction

Coronal mass ejections (CMEs) expel mass and magnetic field from the Sun into the interplanetary (IP) medium, where the observed structures are, in general, called interplanetary CMEs (ICMEs). If certain typical characteristics are present, such as a low plasma β (ratio of the plasma pressure to the magnetic pressure) and a lower proton temperature and a stronger magnetic field than in the surrounding solar wind, which exhibits a smooth and significant rotation, these structures are called magnetic clouds (MCs) (Burlaga *et al.*, 1981).

Observational studies that relate MCs with their sources using different solar signatures have been carried out in the past decade. Some of these efforts have stayed only at a qualitative level, but in recent years quantitative comparisons have also been made. Earlier, Rust (1994) and Bothmer and Schwenn (1994) showed that most MCs associated with filament eruptions had the same magnetic helicity sign possessed by the majority of magnetic features in each solar hemisphere (see *e.g.*, Pevtsov and Balasubramaniam, 2003). Furthermore, the direction of the MC axis was found to be roughly aligned with the disappearing filament (Bothmer and Schwenn, 1994). This result was confirmed later by Marubashi (1997), Bothmer and Schwenn (1998), Zhao and Hoeksema (1998), Yurchyshyn *et al.* (2001, 2005), and Ruzmaikin, Martin, and Hu (2003). More quantitative studies were carried out by Lepping *et al.* (1997), who identified the solar footpoints of the ejected flux ropes in three MCs and concluded that the axial magnetic flux in the cloud was 1.5 times the estimated flux in the probable cloud footpoints and 10% of the magnetic flux in the active region (AR). Leamon *et al.* (2004) derived the MC axial flux, the total current, and the field line twist (number of turns) in 12 MCs and compared these quantities with equivalent ones from their solar sources (but not for a case-to-case basis). These authors concluded that the twist in an MC is created via magnetic reconnection during the eruption.

Other studies quantified the magnetic helicity involved in an eruption taking as a proxy the helicity in an average MC, and comparing it to the different helicity sources in the solar atmosphere (DeVore, 2000; Démoulin *et al.*, 2002; Green *et al.*, 2002; Nindos and Zhang, 2002; Nindos, Zhang, and Zhang, 2003; Mandrini *et al.*, 2004). However, no attempt was made in those studies to measure the decrease of coronal magnetic helicity resulting from an ejection nor to link a particular CME to *in situ* observations of a particular MC. This was done for the first time by Mandrini *et al.* (2005b) and Luoni *et al.* (2005).

Since the magnetic flux contained in a solar ejection is an important quantity that can be used to link coronal to IP observations, we need a solar feature that can be used as proxy for this estimation. Extended intensity decreases in coronal images, called dimmings, are frequently observed in association with front-side CMEs (Thompson *et al.*, 2000). Dimmings were first observed at optical wavelengths in ground-based coronagraph data (Hansen *et al.*, 1974) and in soft X rays by the *Skylab* mission (Rust, 1983). Dimmings have also been

found in *Yohkoh* Soft X-ray Telescope (SXT) data (*e.g.*, Sterling and Hudson, 1997) and in SOHO/Extreme ultraviolet Imaging Telescope (EIT) 195 Å data (*e.g.*, Thompson *et al.*, 1998). The generally accepted physical interpretation of dimmings is that they are primarily a density depletion induced by the eruption of an unstable magnetic configuration, leading to a huge expansion of magnetic loops and the evacuation of plasma along them into the interplanetary space (Hudson, Acton, and Freeland, 1996). Following the eruption, a region of decreased plasma density is left behind (Harrison and Lyons, 2000; Zarro *et al.*, 1999). Evidence directly supporting this interpretation is the study of plasma Doppler motions, using SOHO/Coronal Diagnostic Spectrometer (CDS) data, by Harra and Sterling (2001). Studies of coronal mass loss also strengthen the link between coronal dimming regions and ICMEs (*e.g.*, Sterling and Hudson, 1997; Harrison and Lyons, 2000; Wang *et al.*, 2002; Zhukov and Auchère, 2004). Although large uncertainties are associated with these estimates, such studies do suggest that at least part of the CME mass comes from coronal dimming regions. The spatial correspondence between coronal dimming regions observed in EUV and the angular extent of the associated CME further supports this link (Thompson *et al.*, 2000; Attrill *et al.*, 2007).

Double dimmings, which we will also call core dimmings, are often present on both sides of the erupting configuration. It has been suggested that these dimmings mark the position of the ejected flux rope footpoints (Webb *et al.*, 2000). In the context of this physical interpretation, the eruption of a magnetic flux rope makes up the core magnetic field of the CME, later observed as an ICME or MC. In a model case, the flux rope remains rooted in the dimming regions, at the same time expanding upward in the corona and out into the solar wind. The dimming regions become dark as plasma is evacuated along the very extended ("open") field lines. Recently, Qiu *et al.* (2007) compared the flux in coronal dimmings with the flux in the MCs associated with the eruptive solar events, considering both the flux in the axial and azimuthal MC field components. These authors found that the flux in the dimmings was comparable in an order-of-magnitude sense to the axial MC flux. This result agrees with what is expected in the model case just described.

Following this line, Mandrini *et al.* (2005b) and Attrill *et al.* (2006) have computed the magnetic flux in the two dimming regions associated with two eruptions occurring in bipolar, isolated ARs having different sizes: a small AR and a typical size AR, respectively (see also Webb *et al.*, 2000). In both works it was found that the flux in the dimmings was comparable mainly to the flux in the azimuthal component of the MC field (when one assumes a length compatible with both solar and interplanetary observations). These results led these authors to propose that the ejected flux rope in these cases is formed by successive reconnections in a sheared arcade during the eruption process as described in the following (see also Mandrini *et al.*, 2005a).

Let us describe two extreme cases to clarify the results just discussed. In the first case, a flux rope could be present before an eruption, or it could be formed by magnetic reconnection of a sheared arcade before any significant expansion of the magnetic configuration occurs. Then, in this case, dimmings will be formed only at the footpoints of the flux tube as it expands and erupts. Therefore, the flux measured in the dimmings will be comparable mainly to the MC axial flux. In the second case, which is illustrated in Figure 1, the arcade above the flux rope expands significantly before reconnecting. Then, the dimmings will be formed at the footpoints of the flux rope, and also all along the footpoints of the sheared magnetic arcade as this expansion occurs. Later, the reconnection of the sheared arcade field lines progressively incorporates more flux to the erupting flux tube. In this second case, the flux in the dimming regions will be comparable to the sum of the axial and azimuthal MC flux. This case corresponds to the theoretical two-dimensional model for flux rope eruption

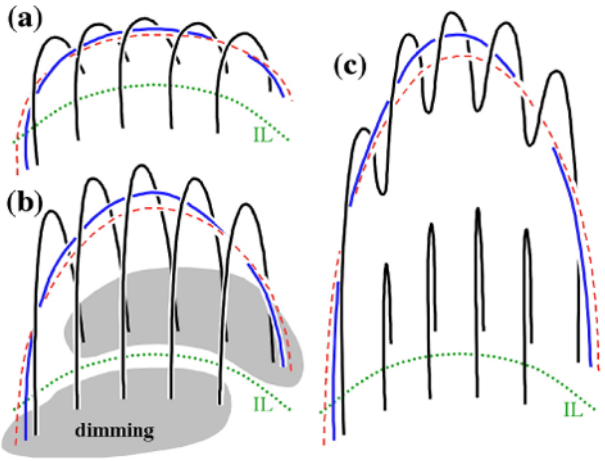

Figure 1 A scenario for flux rope eruption: (a) A flux tube (blue and red lines) is embedded in a sheared arcade (black lines). (b) The arcade above the flux rope expands significantly before reconnecting. Dimmings (light gray areas) are formed at the footpoints of the flux rope and also all along the footpoints of the sheared arcade. (c) The reconnection of the sheared arcade progressively incorporates more flux to the erupting flux tube. In this scenario the magnetic flux in the dimmings should correspond to the sum of the axial and azimuthal flux in the associated MC. The dotted green line is the magnetic photospheric inversion line (IL).

by Lin and Forbes (2000). These authors found that considerable arcade field line stretching can occur before reconnection behind the flux rope adds a significant amount of the arcade flux to the rope. In this model the current sheet formed behind the ascending flux rope can be as long as 3 $R_{\odot}$, whereas in an observational case Pick *et al.* (2005a) have estimated this current sheet length as one tenth of the previous value.

This discussion shows that the comparison of coronal and interplanetary data, associated with the same event, allows us to constrain the CME mechanism. In particular, is the flux rope found in the IP already present in the corona, subsequently becoming unstable and then erupting, or is it formed dominantly during the eruption of an initially sheared arcade by magnetic reconnection? We expect the flux in the dimming regions to be comparable to either the axial flux of the MC or the total flux, respectively, depending on which mechanism is at work.

However, some authors contest the interpretation that dimmings may be the sole source regions of MCs (*e.g.*, Kahler and Hudson, 2001). Indeed, in particularly large scale events occurring in complex and not isolated ARs, the spatial organization of the dimmings can be complicated and their interpretation in terms of magnetic flux involved in the eruption is not straightforward, as we will show in this paper.

We discuss the event, flare and CME, that occurred in AR 10486 (NOAA number) on 28 October 2003. Although this CME is associated with large-scale dimmings, located on either side of the main flaring region, we aim to demonstrate that these dimmings cannot be directly associated with the corresponding cloud found in the IP medium. We combine SOHO/EIT (Delaboudiniere *et al.*, 1995) 195 Å data and Michelson Doppler Imager (SOHO/MDI, Scherrer *et al.*, 1995) magnetic maps to identify and measure the flux in the dimming regions (Section 2). We model the associated MC and compute its magnetic flux using *in situ* observations from the Magnetometer Instrument (MAG, Smith *et al.*, 1998) and the Solar Wind Electron Proton Alpha Monitor (SWEPAM, McComas *et al.*, 1998) aboard the *Advanced Composition Explorer* (ACE, Stone *et al.*, 1998) (Section 3). We then discuss

the apparent incompatibility between the values of the magnetic flux in the coronal dimmings and in the associated MC (Section 4). We conclude that, in certain cases, especially in large-scale events, which interact strongly with surrounding fields, the interpretation of dimmings requires a deeper analysis of the global magnetic configuration, since at least a fraction of the dimmed regions is formed by reconnection between the erupting field and the surrounding magnetic structures (see Attrill *et al.*, 2007).

2. Solar Data Analysis and Results

2.1. Summary of the X17 Flare and CME Properties

The "Halloween" series of intense solar events occurred at the end of 2003, just after solar maximum when the global magnetic structure of the Sun was complex. The eruption that we focus on in this work originated in AR 10486 (S16 E09) on 28 October 2003. AR 10486 arrived at the east solar limb on 23 October 2003 with an already extremely complex magnetic configuration, type beta-gamma-delta, and highly sheared magnetic fields (Zhang *et al.*, 2003; Schmieder *et al.*, 2006; Mandrini *et al.*, 2006). The magnetic flux and field strength were also exceptionally high.

A major two-ribbon X17 flare occurred on 28 October 2003, starting at 11:01 UT with a peak at around 11:10 UT in GOES (*Geostationary Operational Environmental Satellite*) data. It was preceded throughout the previous hour by energy release, evidenced by four flare kernels located on the four main polarities of the AR. Mandrini *et al.* (2006) could link all these kernels by magnetic field lines of the extrapolated photospheric field. They concluded that these brightenings are evidence of a large-scale quadrupolar reconnection process that removed the stabilizing magnetic arcade from above the extremely sheared core. At some point during the evolution, the configuration became unstable, leading to fast energy release and a strong eruption.

The X17 flare was accompanied by the eruption of a filament and by one of the fastest ($\approx$1800 km s^{-1}) halo CMEs registered during the October – November 2003 strong activity period. A fast "coronal wave" signature associated with the eruption was visible in EIT 195 Å data and a Moreton wave was captured in Meudon Observatory Hα data. Both phenomena appeared to propagate across the entire solar disk. The eruption was also associated with the appearance of widespread coronal dimmings. The complexity of the X17 flare on 28 October was analyzed in Hα, radio, and white light images by Pick *et al.* (2005b), and the coronal magnetic structure was linked to the associated MC by Yurchyshyn, Hu, and Abramenko (2005) and Krall *et al.* (2006).

2.2. Extension of the Dimmings

SOHO/EIT 195 Å full-disk images, at approximately 12-minute intervals with a pixel size of 5.26″, are used in this study. Figure 2 shows two EIT images, one before (top panel) and one after (bottom panel) the X17 flare. Comparison of these two unprocessed (neither base nor running difference images) images shows the presence of the dimming regions together with the remnant bright corona over the AR.

To visualize the dimmings clearly, we produce base difference images where the same pre-event image (05:00 UT) is subtracted from all subsequent images. All EIT heliograms are differentially de-rotated to this image time. We use base difference images (as opposed to running difference images) because false dimmings (owing to a change in intensity of a bright structure or displacement of a feature between successive frames) can be created when

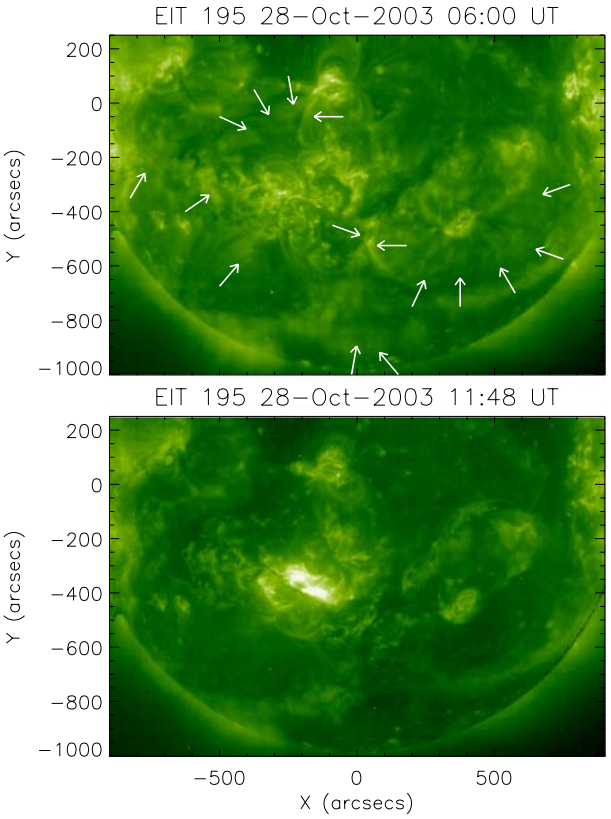

Figure 2 SOHO/EIT 195 Å images before (top panel) and after (bottom panel) the X17 flare. The images show the formation of dimmings around AR 10486 and the remnant bright corona in the AR. The white arrows in the top panel image highlight regions that later show a reduction in intensity when compared to the bottom panel image.

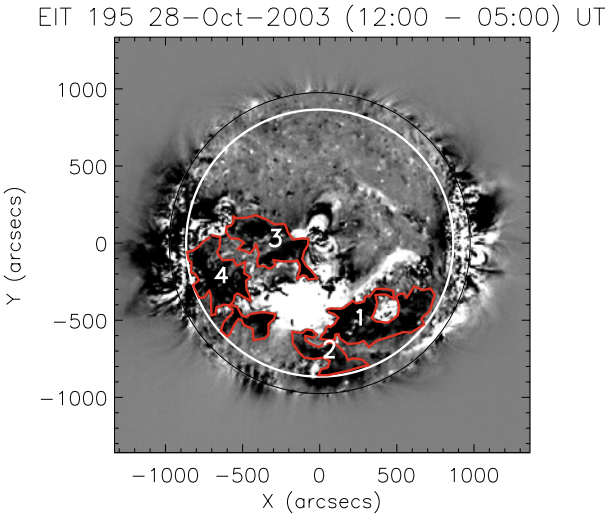

Figure 3 SOHO/EIT 195 Å base difference image (12:00 – 05:00 UT) showing the dimming regions about 1 hour after the start of the X17 flare and associated CME. The dimming regions selected for analysis are numbered and surrounded by red polygonal lines. The white circle is drawn at an angular distance of 60° from the disk center, MDI flux measurements are made within this limit (see Figure 4).

using the running difference method (Chertok *et al.*, 2004; Chertok and Grechnev, 2005). The dimming regions, located on either side of the flaring region, can be easily identified in Figure 3. We have surrounded by red polygonal lines the regions selected for study: the

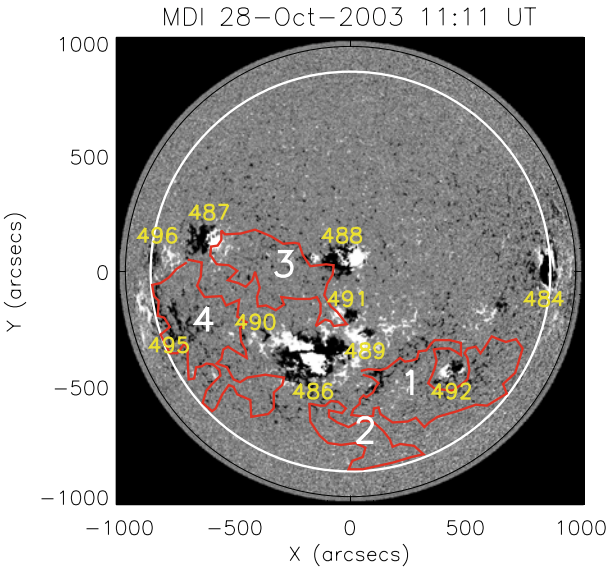

Figure 4 Selected dimming regions overplotted on a deprojected (with radial hypothesis) MDI magnetogram. Black (white) represents the negative (positive) radial magnetic field component. The white circle marks the 60° angular limit up to which MDI measurements are considered reliable. The NOAA numbers of the ARs present on the solar disk at that time have been added in yellow (notice that all numbers should start with 10).

places where the intensity changes abruptly; this gives us a global view of the dimming spatial distribution. A closer inspection shows that many dimmings are present and are, in fact, spread all around AR 10486. Since strong magnetic fields are present in AR 10486, a strong expansion of the erupting field occurred, giving rise to many interactions with the surrounding magnetic configurations.

The spatial distribution of EUV dimmings and "coronal waves" during the strong activity period of October – November 2003 has been also studied by Grechnev *et al.* (2005), combining observations of SOHO/EIT and CORONAS-F/Spectrographic X-Ray Imaging Telescope (SPIRIT, Zhitnik *et al.*, 2002). The location and shape of the dimmings, after the X17 flare and associated CME, derived from SPIRIT are similar to the ones in Figure 3 (compare this figure to Figure 2 in Grechnev *et al.* (2005)).

2.3. Magnetic Flux in the Dimmings

SOHO/MDI level 1.8 full-disk magnetograms with a 96-minute cadence and a pixel size of 1.98″ were used in this study. The data were corrected for radial projection effects by using the standard `zradialize` routine, giving an estimation of the normal field component (B_n), or more precisely the normal flux per unit surface. Since previous studies (*e.g.*, Berger and Lites, 2003; Wang *et al.*, 2003) have shown that MDI significantly underestimates the magnetic flux, we have corrected both the linear and nonlinear response of MDI using the expression $\Phi_{\text{corr.}} = 1.45(\Phi + 0.3\Phi_{|B_n|>1200\text{ G}})$, as indicated in Green *et al.* (2003).

Part of the magnetic flux in the dimmings is due to noise and part forms small-scale connectivities. Such flux does not contribute to the overall net flux of the dimmings. To avoid incorporating this flux into our calculations, we filtered the $|B_n|$ in the dimmings using various lower value thresholds (as in Mandrini *et al.* (2005b); Attrill *et al.* (2006)). Table 1 lists the magnetic flux in the selected regions. Notice that, in contrast to what is found when double or core dimmings are present after an eruption (net flux in each dimming having the opposite sign), the net flux in each of the largest regions (1 and 4) have the same negative sign. Furthermore, the total net flux is strongly negative. The same is true for different threshold field values in Figure 5.

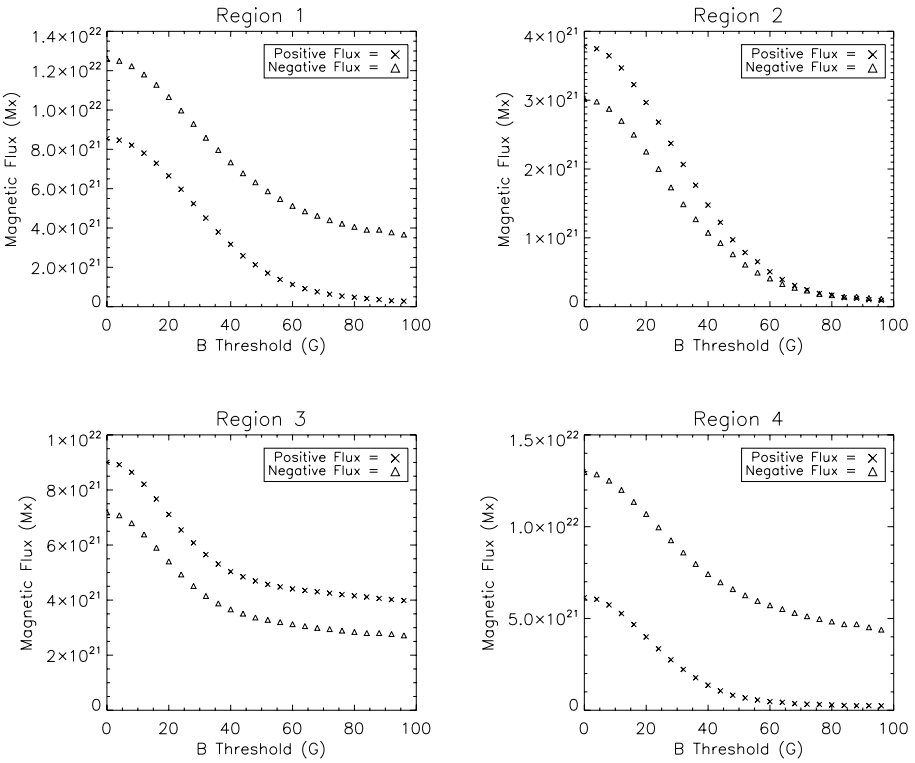

Figure 5 Positive and negative magnetic flux measured through each dimming region (Figure 4) as a function of the magnetic threshold (with the flux of a pixel being counted only if its absolute value is larger than the threshold).

Table 1 Magnetic flux measured through each of the dimming regions defined in Figure 4, with a threshold field value of 20 G (see Figure 5).

Region	Positive flux	Negative flux (10^{21} Mx)	Absolute flux	Net flux
1	6.7	−11.1	17.8	−4.4
2	3.0	−2.3	5.3	0.7
3	7.1	−5.4	12.5	1.7
4	4.0	−11.0	15.0	−7.0

3. Magnetic Cloud Data Analysis and Results

3.1. Boundaries of the Magnetic Cloud

A large magnetic interplanetary structure, exhibiting a strong and rotating field, was observed by the MAG instrument aboard ACE from before midday on 29 October until the early morning of 30 October 2003. The plasma data of this structure were recorded by the SWEPAM instrument. During this period the value of the proton β parameter stayed below 0.1, while the proton temperature was lower than in the surrounding solar wind (Hu *et al.*, 2005). The magnetic field and plasma observations in the Geocentric Solar Ecliptic system

have already been published elsewhere (see ACE data in Figures 1 and 2 and *Wind* observations in Figure 5 of Hu *et al.* (2005)). The *Wind* spacecraft also recorded data at the time of cloud passage, but, since at that time it was exiting the Earth's far magnetotail, these data cannot be directly used in our analysis.

The structure observed by ACE was identified as the MC associated with the midday CME from AR 10486 on 28 October 2003 (Yurchyshyn, Hu, and Abramenko, 2005; Krall *et al.*, 2006). These authors concluded on this association based on the close agreement between the MC axis and the direction of the main AR inversion line and the coincidence between the magnetic helicity sign of the MC and the source AR (both negative).

Several authors have analyzed ACE observations and have reconstructed the cloud structure using different methods and models. Furthermore, different start and end times have also been chosen. Hu *et al.* (2005) and Yurchyshyn, Hu, and Abramenko (2005) used the Grad – Shafranov technique to determine the cloud orientation and physical parameters; these authors took a starting time at 11:17 UT on 29 October and an end time at 03:50 UT on 30 October. Wang *et al.* (2005) and Lynch *et al.* (2005) modeled the cloud observations using the static cylindrical linear force-free model as described by Lepping, Burlaga, and Jones (1990). Wang *et al.* (2005) and Lynch *et al.* (2005) took a cloud duration from 11:00 UT on 29 October to 02:30 UT on 30 October and from 09:00 UT on 29 October to 03:00 UT on 30 October, respectively. Finally, Nieves-Chinchilla, Hidalgo, and Sequeiros (2005) used an expanding non-force-free model with an elliptical cross section. These authors took a much shorter cloud duration from 11:00 UT to 23:10 UT on 29 October.

This variety of cloud borders probably comes from the fact that there are no clear signatures of the start or end of the MC (*e.g.*, shocks and/or discontinuities). After a close inspection of the data, we have taken a cloud duration slightly shorter than that chosen by Hu *et al.* (2005) and Wang *et al.* (2005), choosing a start time at 11:25 UT on 29 October and an end time at 02:00 UT on 30 October 2003. These times correspond to a transition from a fluctuating field to a homogeneous and strong field inbound, and the reverse outbound (Figure 6). We call these boundaries simply "in" and "out."

3.2. Orientation of the Magnetic Cloud

We analyze *in situ* magnetic observations obtained by MAG with 64-second temporal cadence. We define the cloud axis direction, called $\hat{z}_{\text{cloud}}$, using the minimum variance (MV) method (*e.g.*, Sonnerup and Scheible, 1998). The MV method gives a good determination when the impact parameter (p, the minimum distance between the cloud axis and the spacecraft trajectory) is small and the magnetic field components are not significantly asymmetric with respect to the center of the cloud. Gulisano *et al.* (2007) have shown that the MV method gives the MC orientation with a typical error of $\pm 10^{\circ}$ for MCs that can be represented by the classical Lundquist's model (Lundquist, 1950), even in cases where p is larger than 50% of the cloud radius. Previously, for the MC of 29 October 2003, Wang *et al.* (2005) and Lynch *et al.* (2005) found that p was $\approx$40% of the cloud radius.

Furthermore, because the cloud is in expansion (see Figure 6 bottom panel and Section 3.3), the directions derived with the MV method mix two different effects in the variance of the magnetic field **B**: (1) the effect of the coherent rotation of the field (which provides the correct cloud orientation) and (2) the effect of the cloud "aging" (the decrease of the strength of the field with time because of magnetic flux conservation combined with cloud expansion). This latter effect is not associated with the cloud orientation. We apply the MV technique to $\mathbf{B}/B$ to decrease the effect of cloud aging on the orientation found.

We find that the angle between the cloud axis (oriented along **B**) and the ecliptic plane (ecliptic latitude) is -56°. The angle between the projection of the cloud axis on the ecliptic

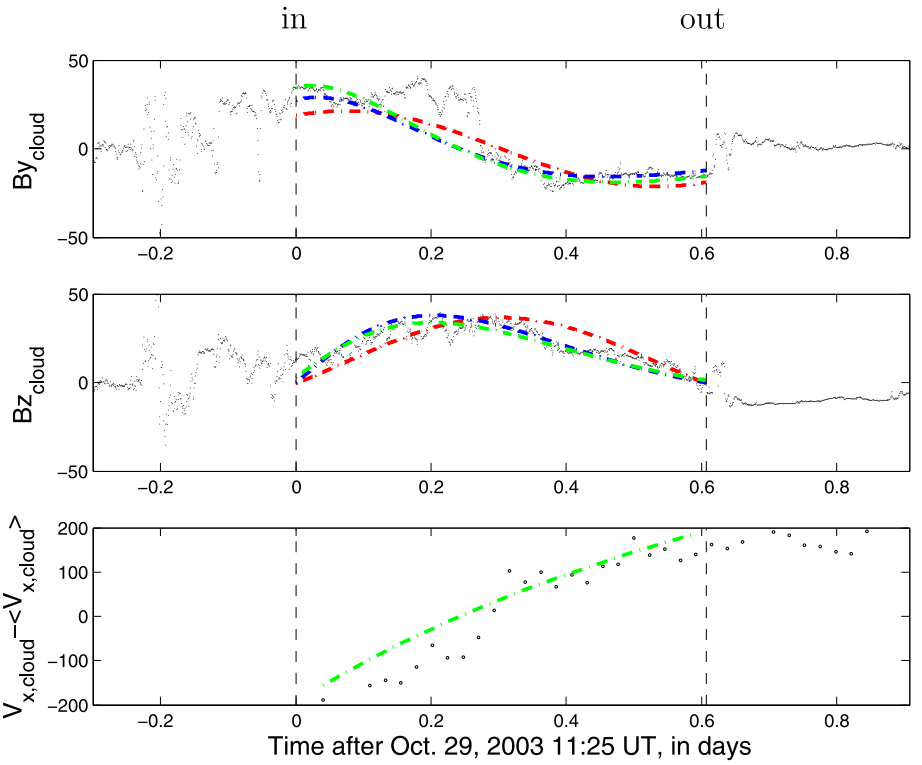

Figure 6 Top and central panels show the $B_{y,\mathrm{cloud}}$ and $B_{z,\mathrm{cloud}}$ components of the magnetic field (measured in nT) in the cloud frame (data from MAG as small dots and fitted curves; see Section 3.4). The red dash-dotted line corresponds to the static Lundquist's model. The blue and green dash-dotted lines correspond to the expansion Lundquist's and the modified expansion Lundquist's models, respectively. The bottom panel shows the observations by SWEPAM (open dots) and the fitted (green dash-dotted line) velocity profile ($V_{x,\mathrm{cloud}} - \langle V_{x,\mathrm{cloud}}\rangle$, in km s^{-1}) for the expansion model [Equation (2)]. Notice the extended data gap at the beginning of this panel. The two vertical lines mark the "in" and "out" boundaries.

plane and the Earth – Sun direction is found to be 197°. This orientation differs at most in 10° either in latitude and longitude from the ones reported by Hu *et al.* (2005) and Lynch *et al.* (2005), despite the significantly different boundaries selected in this latter case (about 2.5 and 1 h for the "in" and "out", respectively). The MC orientation found implies that ACE crossed the MC leg linked to the positive polarity on the Sun (initially in AR 10486).

After applying the MV method to the normalized field data, we rotate the observed magnetic field components to the cloud frame, ($\hat{x}_{\mathrm{cloud}}$, $\hat{y}_{\mathrm{cloud}}$, $\hat{z}_{\mathrm{cloud}}$), as described in Section 2.3 of Dasso *et al.* (2007) (see also Dasso *et al.*, 2006). In this frame, when one considers $p \approx 0$ and a cylindrical structure for the cloud, the vectors are such that $\hat{x}_{\mathrm{cloud}}$, $\hat{y}_{\mathrm{cloud}}$, and $\hat{z}_{\mathrm{cloud}}$ are parallel to the radial, azimuthal, and axial directions, respectively.

3.3. Expansion of the Magnetic Cloud

The SWEPAM instrument experienced several problems during 29 and 30 October because of the extremely high speed solar wind; so several data gaps are present in the observations (Skoug *et al.*, 2004). Still, SWEPAM observations of the proton bulk flow velocity show that this cloud was indeed in expansion (Figure 6).

Table 2 Magnetic fluxes computed for the MC observed on 29 – 30 October 2003 at 1 AU. The first column indicates the fitting model, and the second and third columns show the values of the axial and azimuthal (per unit length) magnetic fluxes, respectively.

Model	F_z (10^{21} Mx)	$F_y\ L^{-1}$ (10^{21} Mx AU^{-1})
Static	3.1	5.7
Expansion	2.9	6.6
Modified	2.8	8.0

We model this expansion by considering an isotropic self-similar case, where all distances are multiplied by a factor $f(t)$, a function of the time t. Since the full MC is observed during a period shorter than the transit time from the Sun, we take only the first linear term in the expansion of $f(t)$ around the MC observing time. This implies that there are no forces acting on any element of the plasma (free expansion; see Dasso *et al.*, 2007). With the previous assumption and since the measured plasma β is low ($0.01 \lesssim \beta \lesssim 0.1$), the MC field is nearly force-free. The function $f(t)$ can be written as

$$f(t) = 1 + (t - t_{\rm in})/T\,, \tag{1}$$

where T is the expansion time, and we select the front boundary "in" for the reference time of distances [$f(t_{\rm in}) = 1$].

The bottom panel in Figure 6 shows with open dots the observed velocity $V_{x,\rm cloud} - \langle V_{x,\rm cloud}\rangle$, where $\langle V_{x,\rm cloud}\rangle = -957$ km s^{-1} is the mean value of the velocity within the cloud. Under the assumption of a low impact parameter, this velocity is approximately the radial velocity with respect to the cloud axis; so as expected for an expanding cloud, it is negative before the spacecraft reaches the cloud axis, and positive afterward.

Taking into account the isotropic expansion, Equation (1), we can obtain the expected velocity profile given by

$$V_x = -V_{\rm c} + V_{\rm c}\,\frac{t - t_{\rm c}}{T + t - t_{\rm in}}\,, \tag{2}$$

where $-V_{\rm c}$ is the velocity of the MC center along $\hat{x}_{\rm cloud}$ and $t_{\rm c}$ is the time when the distance between the spacecraft and the MC axis is minimum (the cloud center for $p = 0$) (see Dasso *et al.*, 2007 for precise details). We take $\langle V_{x,\rm cloud}\rangle$ as a proxy for $V_{\rm c}$. We obtain the expansion time T by fitting Equation (2) to the velocity data. We find $T \approx 29$ h (≈ 1.2 days). The associated CME was initiated just after 11 UT on 28 October. This gives a transit time for the MC center of about 31 h, so very close to the expanding time T (taking into account that the MC is observed over an interval of ± 7 h). This agreement of the durations is compatible with a linear expansion in time, not only during the observing time but also for the full transit from the Sun [since $f(t) = 0$ for $t = t_{\rm in} - T$ in Equation (1)].

Considering this velocity profile and assuming a nearly constant mean velocity for the cloud during the spacecraft crossing and a low p, we can estimate the MC radius. The full MC crossing corresponds to a size $R_{\rm in} + R_{\rm out} = R_{\rm in}[1 + f(t_{\rm out})]$. This gives $R_{\rm in} = 0.13$ AU and $R_{\rm out} = 0.20$ AU and thus a radial expansion of 42% ($2\frac{R_{\rm out} - R_{\rm in}}{R_{\rm out} + R_{\rm in}} = 0.42$) during the observation period. If we have not taken into account the expansion, we would have found a radius that is just the mean value between $R_{\rm in}$ and $R_{\rm out}$ (since the total length crossed is given by the observed velocity profile).

3.4. Magnetic Flux in the Magnetic Cloud

We quantify the magnetic flux in the cloud by fitting three models to the observations. We consider the classical static Lundquist's model (Lundquist, 1950) and two self-similar ex-

pansion cases. For the expansion cases, the distances are scaled by the factor $f(t)$ and the field by a factor $f^{-2}(t)$. These two expansion cases, which we call the expansion Lundquist's model (see Shimazu and Vandas, 2002) and the modified expansion Lundquist's model, are described in Dasso *et al.* (2007). In the expansion Lundquist's model both the azimuthal and axial components of the field depend on the same free parameter, whereas in the modified expansion model the dependence is different for the two components of the field, so the model has two free parameters. Even though the cloud orientation can be found quite precisely using the MV method, assuming a low p implies an underestimation of the magnetic flux values (because the magnetic field measured is lower than for a central crossing and the MC radius is underestimated). We will not present a detailed analysis of the cloud structure; our aim is to give a lower bound estimate of the cloud flux to compare it with the magnetic flux in the dimmings.

The top and central panels in Figure 6 show the curves for the different fittings: static, expansion, and modified expansion Lundquist's models (red, blue, and green dash-dotted lines, respectively). As seen in the top panel, none of the models can fit the structure observed between 11:31 UT and 11:43 UT on 29 October. However, the modified expansion Lundquist's model is the one that best reproduces the asymmetric beginning and end of the cloud for $B_{y,\mathrm{cloud}}$. For $B_{z,\mathrm{cloud}}$, both expansion models closely follow the data; the static model is the one that gives the worst fitting.

From the fitted parameters we compute the axial (F_z) and azimuthal (F_φ) magnetic fluxes, as done in Dasso *et al.* (2007). Our results are listed in Table 2. We estimate the cloud fluxes, taking the range given by the three models, as 2.8×10^{21} Mx $\leq F_z \leq 3.1 \times 10^{21}$ Mx and 5.7×10^{21} Mx/AU $\leq F_y/L \leq 8.0 \times 10^{21}$ Mx/AU.

Analyzing SWEPAM observations of suprathermal electrons, Skoug *et al.* (2004) found the presence of counterstreaming electron flows for a period of time within the MC, though there were periods when electron measurements were unreliable. This would imply that the cloud is anchored to the Sun at both ends when observed at 1 AU; so the MC length should be at least 2 AU. Considering this minimum length and summing F_z and F_y gives a total cloud flux in the range 14×10^{21} Mx $\leq F_{\mathrm{MC}} \leq 19 \times 10^{21}$ Mx. It is noteworthy that this value is a lower bound estimate for the MC flux, as has already been discussed.

4. Linking Coronal and Interplanetary Results

4.1. Do the Magnetic Fluxes of Dimmings and MCs Match?

Even though the two most extended dimmings (dimmings 1 and 4; see Figures 3 and 4) appear on either side of AR 10486, they do not present the typical characteristics of double or core dimmings. The latter are present at both sides of the eruptive magnetic configuration and have magnetic net fluxes of opposite signs with approximately the same absolute values (see Section 1).

For the event on 28 October 2003, we find that dimmings 1 and 4 have net negative fluxes, whereas the net fluxes in the others (dimmings 2 and 3) are positive. Furthermore, if we add the net fluxes in dimmings 1 and 4 and those of 2 and 3, the latter value is one order of magnitude lower (*i.e.* the total net flux is not balanced). Indeed both dimmings 2 and 3 are located above quiet Sun regions where the positive flux only dominates slightly (see Figure 5, showing positive and negative flux curves that are close together). The net result is that all the flux covered by the dimming regions has a strong negative imbalance.

Dimming 1 extends above the negative polarity of the decaying AR by which AR 10486 is bounded to the west. It also encompasses the negative field surrounding AR 10492. Both

these negative fields are not balanced by the less intense positive fields within the dimming (Figure 4). However, dimming 4 extends mainly above the negative field in AR 10495. There is also an important dimming close to dimming 4, lying above the eastern limb (Figure 3). This dimming is located over the positive flux part of AR 10495. Its location does not allow us to estimate its flux, but in view of its location the flux is expected to be dominantly positive and to have a comparable magnitude to the flux found in dimming 4. Since the following polarity of AR 10486 is positive, and the erupting flux rope is rooted there (see Mandrini *et al.*, 2006), at least at the beginning of the eruption, positive dimmings both there and at some location to the east are expected. The dimming above the eastern limb is the only one that plausibly has enough positive flux to coincide with the positive footpoint of the erupting magnetic configuration!

The net flux in dimming 1 is $\approx -4.4 \times 10^{21}$ Mx, this value is close to the axial MC flux range $(2.8-3.1) \times 10^{21}$ Mx. This suggests that dimming 1 could probably correspond to the original negative MC footpoint in the classical scenario in which an already existing flux tube expands and erupts. However, we argue that this cannot be the case since the eruption occurred inside AR 10486 and dimming 1 is located far to the west of the region; furthermore, we do not find the corresponding associated positive dimming. However, if the flux rope is dominantly formed by reconnection during the eruption, we have to compare the dimming flux to the total MC flux observed in the interplanetary space (Section 1 and Figure 1). The total negative net flux in dimmings 1 and 4 ($\approx 11 \times 10^{21}$ Mx) is close to the lower limit of the total MC flux for the estimated cloud length, 14×10^{21} Mx $\leq F_{\mathrm{MC}} \leq 19 \times 10^{21}$ Mx. However, considering that this estimation is a lower bound as discussed in Section 3.4, we conclude that the flux in the dimmings identified on the disk does not match the total flux in the cloud and, in view of their spatial distribution and net flux, the observed dimmings (1 to 4) do not represent the initial footpoints of the ejected magnetic configuration (initial flux and surrounding arcade).

4.2. Origin of the Dimmings on the 28 October Event

Besides core dimmings, there is another type of dimming, more widespread, that corresponds to the spatial extent of CMEs detected in coronagraph data (Thompson *et al.*, 2000). We call these secondary dimmings. Our results in the previous paragraphs are an indication that, in this particular event, we do not observe the deep core dimmings, but rather secondary dimmings, the origin of which we discuss in the following.

Recently, Attrill *et al.* (2007) have proposed a new mechanism where driven magnetic reconnection between the outer edge of an expanding CME magnetic field and quiet-Sun magnetic loops can generate the observed diffuse bright fronts that constitute the leading edge of "coronal EIT waves". It is noteworthy that the magnetic configuration of surrounding ARs can replace some of the quiet-Sun loops of the events they studied (which occurred close to solar minimum). In this scenario, the presence of widespread secondary dimmings behind the diffuse bright front is a natural consequence of the driven reconnections.

Could this mechanism be responsible for the dimmings observed in this 28 October 2003 event? Figure 7 illustrates the way in which dimmings 1 and 4 could have been formed. As the main filament in AR 10486 erupts, the magnetic field of the AR expands and to the west encounters a nearby filament channel between the positive and negative polarities (where dimming 1 lies; Figure 7a) of the decaying AR preceding AR 10486. To the east, quiet-Sun fields are encountered (where dimming 4 lies; Figure 7a). The expanding CME magnetic loops reconnect with the favorably oriented loops that are encountered both to the west and the east. Magnetic reconnection creates two new sets of connections. One

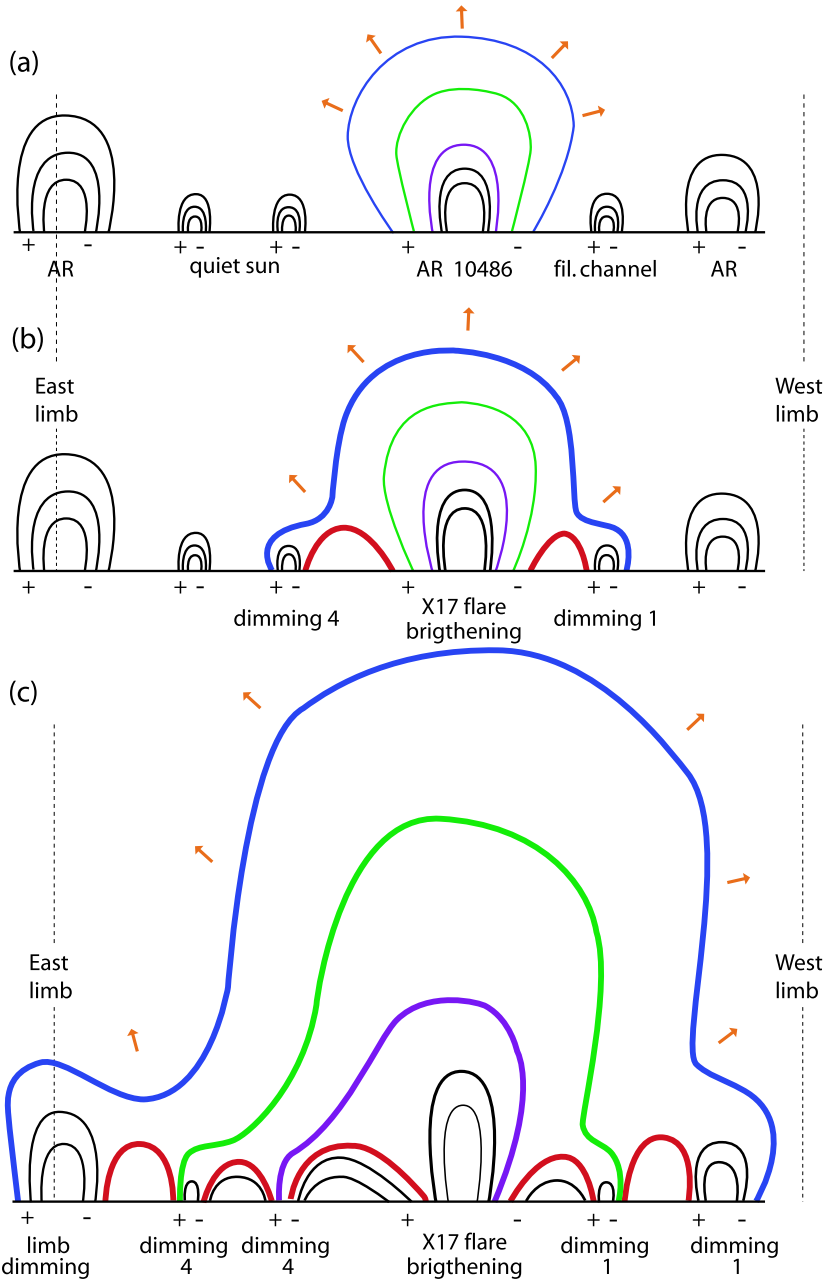

Figure 7 Reconnection of the expanding CME field configuration with the surrounding bipoles: dimming spreading (mechanism proposed by Attrill *et al.* (2007), applied to the 28 October 2003 event). (a) The CME liftoff. AR 10486 is represented by five field lines; nearby bipoles are represented with three black field lines. (b) and (c) By successive reconnections the outer shell of the CME expanding magnetic field is progressively rooted in more distant regions. This creates the spreading of the dimmings to larger spatial scales. In these figures the just reconnected field lines are thicker (and set to red for the short loops).

set is formed by small loops (red field lines in Figure 7b). These reconnected loops imply brightenings owing to chromospheric evaporation (these loops constitute the bright front surrounding the core dimmings of the AR, as shown by Attrill *et al.* (2007)). The second result of magnetic reconnection is to form long loops (blue field line in Figure 6b), still belonging to the erupting magnetic configuration but with new, displaced footpoints (they form the diffuse leading edge front of the "coronal wave"). Dimmings are associated with these large loops as the plasma, initially contained in the surrounding loops, becomes free to expand into the larger volume created by the long (blue) loop.

This process is repeated many times as the continuing lateral expansion of the CME core drives progressively new reconnections (see Figure 7c). To the west, the expanding structure encounters and reconnects with the favorably orientated magnetic loops in AR 10492 (represented by the three black field lines on the right side of Figures 7a and 7b). To the east, reconnection with favorably oriented quiet-Sun loops continues until the still expanding CME encounters loops belonging to AR 10495 (represented by the three black field lines on the left side of Figures 7a and 7b). The removal by reconnection of the outer set of loops in AR 10495 produces dimmings on both polarities; this is the main reason why dimming 4 has a net negative flux. This continuous step-like reconnection process results in the spread of the secondary dimming 4 and the appearance of dimming over the east limb.

The secondary dimmings 2 and 3 are understood to form by the same mechanism. Reconnection occurs in these regions with loops of the quiet Sun in a more mixed field environment, with some new features as follows.

Dimming 2 extends south to the positive polar coronal hole. There the negative expanding edge of the CME configuration reconnects with "open" positive field lines, creating small reconnected loops (see Benevolenskaya, 2004). The reconnection region progressively shifts its location along the inversion line so that a "zipper-like", moving brightening is observed (see also Attrill *et al.*, 2006). These interchange reconnections (Crooker, Gosling, and Kahler, 2002) also imply a partial, but true, disconnection of this southern part of the negative leg of the CME from the Sun. The disconnection of the negative leg of this part of the CME field implies that the other (positive) end of the field is "open", leading to dimming in the positive leg. This process may well contribute to the formation of dimming region 3.

For dimming 3, besides the latter mechanism, two other mechanisms contribute to dimming formation: quiet-Sun reconnections, as proposed by Attrill *et al.* (2007), and the "disappearance" of bright loops connecting AR 10496 to the northern AR 10487, and AR 10491 to AR 10488, as described in other events by Delannée (2000).

4.3. Complexity of Large-Scale Events

In summary, the basic skeleton of a CME consists of the upward extension of the erupting configuration and the formation of a pair of core dimmings. However, none of the observed dimmings on the 28 October event can be associated with such core dimmings. Instead, we have identified them as secondary dimmings, as proposed by Attrill *et al.* (2007). The strong energy release during the X17 flare in AR 10486 led to strong chromospheric evaporation and the formation of dense and bright coronal loops (see, *e.g.*, the movies included in Mandrini *et al.* (2006)). The strong emission of these loops, combined with the spreading of the saturated signal, covers most of AR 10486. Any core dimming, strong as it could be, is masked by the intense emission of the flaring region so that none of the expected core dimmings can be observed. We expect that this is a general property of very strong events.

Next, let us consider the case of less energetic flares. The magnetic reconnection process that creates the secondary dimmings should conserve magnetic flux. Then, when we observe

both core and secondary dimming regions, we would expect that their total flux divided by 2 should equate to the total flux in the associated MC. However, the formation of secondary dimmings is a time-dependent complex process. As the flux connectivity is transferred from the core dimmings to the surrounding regions, the disappearance of the dimmings in the core takes time (the time needed to replenish the corona with plasma). A delay, plausibly smaller, can be also expected in the formation of the secondary dimmings (the time needed for the plasma to be evacuated). Moreover, brightenings are expected to form very close to the dimmings and only the deeper part of the dimming is expected to be detectable.

The dynamic process discussed here leads to uncertainties in defining the boundary of such secondary dimmings at a given time; so, there are uncertainties when adding the magnetic flux of the core and secondary dimmings at any given time. This added flux is a proxy of the total magnetic flux associated with the expanded field lines, but there are both thermodynamic and kinematic delays that can distort this estimation. Moreover, these uncertainties grow with the number of reconnecting steps needed to create the secondary dimmings. Therefore, direct comparisons between the magnetic flux in the dimmings and the total flux of the associated MC are difficult in large-scale events (with a large flare and/or a large lateral expansion and reconnection with many bipoles).

5. Conclusion

Previous work has suggested that coronal dimming regions at either side of the flare loops mark the position of the erupting flux rope footpoints (Webb *et al.*, 2000). This was later confirmed by Mandrini *et al.* (2006) and Attrill *et al.* (2006) but in a scenario in which the flux rope found in the interplanetary medium was mostly formed by reconnection during the eruption process. During the ejection of the magnetic configuration (which makes up the associated CME), magnetic loops drastically expand. The plasma can expand upward into this larger volume, forming dimming regions at these locations. However, in large-scale (intense) events such a simple interpretation encounters difficulties because of the presence of brightenings (owing to the flare and often a global-scale "EIT coronal wave" and associated persistent brightenings) and because of reconnection of the erupting field with the surrounding environment, as summarized in the following.

First, the large energy release in the flare leads to strong chromospheric evaporation and the formation of dense and bright coronal loops. The core dimmings, located in the vicinity of these central brightenings, can be (at least partly) obscured by the flare brightenings. The X17 flare, analyzed in this paper, was so intense that we can observe none of the expected core dimmings.

Second, a strong magnetic field in the AR means that the erupting field has a significant magnetic pressure. This implies a strong expansion of the erupting field, not only vertically but also laterally over neighboring quiet-Sun regions and ARs. As a result, magnetic reconnection is expected in most cases (*i.e.*, cases with almost parallel fields are rare). These reconnections imply the formation of new brightenings (contributing to the "EIT wave" phenomena), as well as a reorganization of the magnetic connectivities, which enables the spread of the dimmings over a region much larger than that of the original eruption (Attrill *et al.*, 2007). These reconnections imply that CMEs become large scale even in the low corona, as evidenced by radio observations at metric wavelengths (Pick *et al.*, 2005b) and by the large spatial extent of CME-associated limb dimmings observed in EIT 195 Å (Thompson *et al.*, 2000).

Third, a large event can also induce strong effects in neighboring active regions, for example, the destabilization of interconnecting loops (between the initial eruption site and

surrounding regions) and/or inside nearby ARs (Delannée, Hochedez, and Aulanier, 2007). Destabilization of surrounding structures can be recognized by the loop shape of the dimmings and by comparing the locations of the dimmings (difference images) with EUV and X-ray direct images where coronal loop structures can be identified before the CME.

Finally, other biases are present since the observations give only the total intensity integrated along the line of sight. In particular, brightenings and dimmings can be mixed up along the same line of sight. This bias is expected to be important since the physics of the eruption involves the coupled formation of brightenings and dimmings (Attrill *et al.*, 2007). This mixing effect increases as one observes farther away from the disk center. In large events, where signatures extend to a large fraction of the solar disk, this effect cannot be avoided, even by analyzing events that start close to the disk center.

We conclude that a careful analysis of the origin of the various dimmings is required before their magnetic flux can be compared to that of the associated interplanetary MC. This is especially true in large events because of the failure in observing core dimmings and the biases induced by mixing brightenings and dark regions. This is also present in medium and small events because of the interaction of the expanding field with neighboring fields (both for quiet Sun and nearby ARs).

Acknowledgements We thank the SOHO/EIT and SOHO/MDI consortia for their data. SOHO is a project of international cooperation between ESA and NASA. This work was partially supported by the Argentinean grants UBACyT X329, PIP 6220 (CONICET), and PICTs 03-12187 and 03-14163 (ANPCyT). L.v.D.G. acknowledges the Hungarian government grant OTKA 048961. C.H.M. and P.D. acknowledge financial support from CNRS (France) and CONICET (Argentina) through their cooperative science program (No. 20326). The authors thank the organization of the Sun – Earth workshop at MSSL that allowed the conception of this work. S.D. and C.H.M. are members of the Carrera del Investigador Científico. M.S.N. is a fellow of CONICET. G.D.R.A. is grateful to PPARC for support.

References

Attrill, G., Nakwacki, M.S., Harra, L.K., van Driel-Gesztelyi, L., Mandrini, C.H., Dasso, S., Wang, J.: 2006, *Solar Phys.* **238**, 117.
Attrill, G.D.R., Harra, L.K., van Driel-Gesztelyi, L., Démoulin, P.: 2007, *Astrophys. J.* **656**, L101.
Benevolenskaya, E.E.: 2004, *Astron. Astrophys.* **428**, L5.
Berger, T.E., Lites, B.W.: 2003, *Solar Phys.* **213**, 213.
Bothmer, V., Schwenn, R.: 1994, *Space Sci. Rev.* **70**, 215.
Bothmer, V., Schwenn, R.: 1998, *Ann. Geophys.* **16**, 1.
Burlaga, L., Sittler, E., Mariani, F., Schwenn, R.: 1981, *J. Geophys. Res.* **86**, 6673.
Chertok, I.M., Grechnev, V.V.: 2005, *Solar Phys.* **229**, 95.
Chertok, I.M., Grechnev, V.V., Hudson, H.S., Nitta, N.V.: 2004, *J. Geophys. Res.* **109**(A2), A02112.
Crooker, N.U., Gosling, J.T., Kahler, S.W.: 2002, *J. Geophys. Res.* **107**(A2), 1028.
Démoulin, P., Mandrini, C.H., van Driel-Gesztelyi, L., Lopez Fuentes, M.C., Aulanier, G.: 2002, *Solar Phys.* **207**, 87.
Dasso, S., Mandrini, C.H., Démoulin, P., Luoni, M.L.: 2006, *Astron. Astrophys.* **455**, 349.
Dasso, S., Nakwacki, M.S., Démoulin, P., Mandrini, C.H.: 2007, *Solar Phys.*, in press.
Delaboudiniere, J.P., Artzner, G.E., Brunaud, J., Gabriel, A.H., Hochedez, J.F., Millier, F., *et al.*: 1995, *Solar Phys.* **162**, 291.
Delannée, C.: 2000, *Astrophys. J.* **545**, 512.
Delannée, C., Hochedez, J.F., Aulanier, G.: 2007, *Astron. Astrophys.* **465**, 603.
DeVore, C.R.: 2000, *Astrophys. J.* **539**, 944.
Grechnev, V.V., Chertok, I.M., Slemzin, V.A., Kuzin, S.V., Ignat'ev, A.P., Pertsov, A.A., Zhitnik, I.A., Delaboudinière, J.P., Auchère, F.: 2005, *J. Geophys. Res.* **110**(A9), A09S07.
Green, L.M., López Fuentes, M.C., Mandrini, C.H., Démoulin, P., van Driel-Gesztelyi, L., Culhane, J.L.: 2002, *Solar Phys.* **208**, 43.
Green, L.M., Démoulin, P., Mandrini, C.H., van Driel-Gesztelyi, L.: 2003, *Solar Phys.* **215**, 307.
Gulisano, A.M., Dasso, S., Mandrini, C.H., Démoulin, P.: 2007, *Adv. Space Res.*, in press.

Hansen, R.T., Garcia, C.J., Hansen, S.F., Yasukawa, E.: 1974, *Publ. Astron. Soc. Pacific* **86**, 500.
Harra, L.K., Sterling, A.C.: 2001, *Astrophys. J.* **561**, L215.
Harrison, R.A., Lyons, M.: 2000, *Astron. Astrophys.* **358**, 1097.
Hu, Q., Smith, C.W., Ness, N.F., Skoug, R.M.: 2005, *J. Geophys. Res.* **110**(A9), A09S03.
Hudson, H.S., Acton, L.W., Freeland, S.L.: 1996, *Astrophys. J.* **470**, 629.
Kahler, S.W., Hudson, H.S.: 2001, *J. Geophys. Res.* **106**, 29239.
Krall, J., Yurchyshyn, V.B., Slinker, S., Skoug, R.M., Chen, J.: 2006, *Astrophys. J.* **642**, 541.
Leamon, R.J., Canfield, R.C., Jones, S.L., Lambkin, K., Lundberg, B.J., Pevtsov, A.A.: 2004, *J. Geophys. Res.* **109**, A05106.
Lepping, R.P., Burlaga, L.F., Jones, J.A.: 1990, *J. Geophys. Res.* **95**, 11957.
Lepping, R.P., Szabo, A., DeForest, C.E., Thompson, B.J.: 1997, In: Wilson, A. (ed.) *Correlated Phenomena at the Sun, in the Heliosphere and in Geospace*, *ESA SP-415*, 163.
Lin, J., Forbes, T.G.: 2000, *J. Geophys. Res.* **105**, 2375.
Lundquist, S.: 1950, *Ark. Fys.* **2**, 361.
Luoni, M.L., Mandrini, C.H., Dasso, S., van Driel-Gesztelyi, L., Démoulin, P.: 2005, *J. Atmos. Solar Terr. Phys.* **67**, 1734.
Lynch, B.J., Gruesbeck, J.R., Zurbuchen, T.H., Antiochos, S.K.: 2005, *J. Geophys. Res.* **110**, A08107.
Mandrini, C.H., Démoulin, P., van Driel-Gesztelyi, L., Green, L.M., López Fuentes, M.C.: 2004, *Astrophys. Space Sci.* **290**, 319.
Mandrini, C.H., Dasso, S., Luoni, M.L., Pohjolainen, S., Démoulin, P., van Driel-Gesztelyi, L.: 2005a, In: Innes, D.E., Lagg, A., Solanki, S.A. (eds.) *Chromospheric and Coronal Magnetic Fields*, *ESA SP-596*, 205.
Mandrini, C.H., Pohjolainen, S., Dasso, S., Green, L.M., Démoulin, P., van Driel-Gesztelyi, L., Copperwheat, C., Foley, C.: 2005b, *Astron. Astrophys.* **434**, 725.
Mandrini, C.H., Démoulin, P., Schmieder, B., Deluca, E., Pariat, E., Uddin, W.: 2006, *Solar Phys.* **238**, 293.
Marubashi, K.: 1997, In: Crooker, N., Joselyn, J.A., Feynman, J. (eds.) *Coronal Mass Ejections*, *Geophys. Monograph*, Vol. 99, American Geophysical Union, 147.
McComas, D.J., Bame, S.J., Barker, P.L., Delapp, D.M., Feldman, W.C., Gosling, J.T., *et al.*: 1998, *Geophys. Res. Lett.* **25**, 4289.
Nieves-Chinchilla, T., Hidalgo, M.A., Sequeiros, J.: 2005, *Solar Phys.* **232**, 105.
Nindos, A., Zhang, H.: 2002, *Astrophys. J.* **573**, L133.
Nindos, A., Zhang, J., Zhang, H.: 2003, *Astrophys. J.* **594**, 1033.
Pevtsov, A.A., Balasubramaniam, K.S.: 2003, *Adv. Space Res.* **32**, 1867.
Pick, M., Démoulin, P., Krucker, S., Malandraki, O., Maia, D.: 2005a, *Astrophys. J.* **625**, 1019.
Pick, M., Malherbe, J.M., Kerdraon, A., Maia, D.J.F.: 2005b, *Astrophys. J.* **631**, L97.
Qiu, J., Hu, Q., Howard, T.A., Yurchyshyn, V.B.: 2007, *Astrophys. J.* **659**, 758.
Rust, D.M.: 1983, *Space Sci. Rev.* **34**, 21.
Rust, D.M.: 1994, *Geophys. Res. Lett.* **21**, 241.
Ruzmaikin, A., Martin, S., Hu, Q.: 2003, *J. Geophys. Res.* **108**(A2), 1096.
Scherrer, P.H., Bogart, R.S., Bush, R.I., Hoeksema, J.T., Kosovichev, A.G., Schou, J., *et al.*: 1995, *Solar Phys.* **162**, 129.
Schmieder, B., Mandrini, C.H., Démoulin, P., Pariat, E., Berlicki, A., Deluca, E.: 2006, *Adv. Space Res.* **37**, 1313.
Shimazu, H., Vandas, M.: 2002, *Earth, Planets, Space* **54**, 783.
Skoug, R.M., Gosling, J.T., Steinberg, J.T., McComas, D.J., Smith, C.W., Ness, N.F., Hu, Q., Burlaga, L.F.: 2004, *J. Geophys. Res.* **109**(A09), A09102.
Smith, C.W., L'Heureux, J., Ness, N.F., Acuña, M.H., Burlaga, L.F., Scheifele, J.: 1998, *Space Sci. Rev.* **86**, 613.
Sonnerup, B.U.O., Scheible, M.: 1998, *ISSI Science Report, Sr-001*, Kluwer Academic.
Sterling, A.C., Hudson, H.S.: 1997, *Astrophys. J.* **491**, L55.
Stone, E.C., Frandsen, A.M., Mewaldt, R.A., Christian, E.R., Margolies, D., Ormes, J.F., Snow, F.: 1998, *Space Sci. Rev.* **86**, 1.
Thompson, B.J., Cliver, E.W., Nitta, N., Delannée, C., Delaboudinière, J.P.: 2000, *Geophys. Res. Lett.* **27**, 1431.
Thompson, B.J., Plunkett, S.P., Gurman, J.B., Newmark, J.S., St. Cyr, O.C., Michels, D.J., Delaboudinière, J.P.: 1998, *Geophys. Res. Lett.* **25**, 2461.
Wang, J., Zhou, G., Wang, Y., Song, L.: 2003, *Solar Phys.* **216**, 143.
Wang, T., Yan, Y., Wang, J., Kurokawa, H., Shibata, K.: 2002, *Astrophys. J.* **572**, 580.
Wang, Y., Ye, P., Zhou, G., Wang, S., Wang, S., Yan, Y., Wang, J.: 2005, *Solar Phys.* **226**, 337.
Webb, D.F., Lepping, R.P., Burlaga, L.F., DeForest, C.E., Larson, D.E., Martin, S.F., Plunkett, S.P., Rust, D.M.: 2000, *J. Geophys. Res.* **105**, 27251.

Yurchyshyn, V., Hu, Q., Abramenko, V.: 2005, *Space Weather* **3**, 8.
Yurchyshyn, V.B., Wang, H., Goode, P.R., Deng, Y.: 2001, *Astrophys. J.* **563**, 381.
Zarro, D.M., Sterling, A.C., Thompson, B.J., Hudson, H.S., Nitta, N.: 1999, *Astrophys. J.* **520**, L139.
Zhang, H.Q., Bao, X.M., Zhang, Y., Liu, J.H., Bao, S.D., Deng, Y.Y., *et al.*: 2003, *Chin. J. Astron. Astrophys.* **3**, 491.
Zhao, X.P., Hoeksema, J.T.: 1998, *J. Geophys. Res.* **103**(A2), 2077.
Zhitnik, I.A., Bougaenko, O.I., Delaboudiniere, J.P., Ignatiev, A.P., Korneev, V.V., Krutov, V.V., *et al.*: 2002, In: Kuijpers, J. (ed.) *Solar Variability: From Core to Outer Frontiers*, *ESA SP-506*, 915.
Zhukov, A.N., Auchère, F.: 2004, *Astron. Astrophys.* **427**, 705.